Available online at www.sciencedirect.com

SciVerse ScienceDirect

Ceramics International 39 (2013) 6681–6688

CERAMICS INTERNATIONAL

www.elsevier.com/locate/ceramint

Carboxylic acids and polyethylene glycol assisted synthesis of nanocrystalline nickel ferrites

A.S. Nikolić[a], N. Jović[b], J. Rogan[c], A. Kremenović[b,d], M. Ristić[e], A. Meden[f], B. Antić[b,*]

[a]Faculty of Chemistry, University of Belgrade, Studentski trg 12–16, 11000 Belgrade, Serbia
[b]The "Vinča" Institute of Nuclear Sciences, University of Belgrade, POB 522, 11001 Belgrade, Serbia
[c]Faculty of Technology and Metallurgy, University of Belgrade, Karnegijeva 4, 11000 Belgrade, Serbia
[d]Laboratory of Crystallography, Faculty of Mining and Geology, University of Belgrade, Djusina 7, 11001 Belgrade, Serbia
[e]Division of Materials Chemistry, Ruđer Bošković Institute, POB 180, HR-10002 Zagreb, Croatia
[f]University of Ljubljana, Faculty of Chemistry and Chemical Technology, 1000 Ljubljana, Slovenia

Received 18 November 2012; received in revised form 25 November 2012; accepted 29 January 2013
Available online 10 February 2013

Abstract

Different synthesis methods for the preparation of nanocrystalline nickel ferrites are reported: the thermal decomposition of precursors, made of: (*i*) metal-nitrate salts with carboxylic acids (citric, malonic and tartaric), and (*ii*) metal-nitrate salts and polyethylene glycol (PEG), in the presence of potassium chloride as a capping agent. The as-prepared gel precursors were characterized by TGA/DTA, while the samples obtained after annealing at 450 °C were investigated by FTIR, FESEM, XRD and Mössbauer spectroscopy. Regardless of the type of carboxylic acid used, nanocrystallites prepared by (*i*) method are similar in size (11–16 nm), while the method (*ii*) gives crystallites ~33 nm in size with negligible microstrain. The differences in the lattice parameter, ranging from 8.3369(2) to 8.3574(2) Å, result from cation distribution, nonstoichiometry and structural imperfections in the nickel ferrite nanoparticles. The Mössbauer spectra analysis indicates existence of large distortions of tetrahedral and octahedral sites in these spinel compounds.

Keywords: D. Ferrite; Nanoparticles; Synthesis; Characterization

1. Introduction

Recently the great effort has been done to invent new, and to modify existing synthesis procedure in order to produce nanomaterials with improved performances. This becomes important for industrial ceramics where some needs are required (e.g. high magnetization, resistivity, coercivity, etc.). Concerning biomedical application of magnetic nanomaterials it is important to have narrow particle size distribution, superparamagnetic behaviour at room temperature and Currie temperature of cc. 40 °C (for hyperthermia treatment) [1]. The relationship between synthesis and applications is based on the fact that synthesis procedure determines structural and microstructural characteristics of materials such as cation distribution, particle size, microstrain, kinds of defects. These structural characteristics further have favorable influence in physical (magnetical, electrical, optical) properties of the applied materials.

Having in mind an extremely wide range of their application [2], in this paper we studied nanosized nickel ferrites. These soft ferrites are usually used in magnetic recording media, catalyst, for microwave applications, pigment, etc. [2]. They crystallize in spinel structure (space group *Fd*-3*m*), where cations are distributed between tetrahedral (8*a*) and octahedral (16*d*) sites. This distribution critically determines magnetic behavior because of superexchange mechanism based on interactions between magnetic ions via oxygen [3]. The distribution is usually presented by the structural formula $(Ni^{2+}_{1-\alpha}Fe^{3+}_{\alpha})_{8a}[Fe^{3+}_{2-\alpha}Ni^{2+}_{\alpha}]_{16d}$,where α is denoted as the degree of

*Corresponding author. Tel./fax: +381118065829.
E-mail address: bantic@vinca.rs (B. Antić).

0272-8842/$ - see front matter © 2013 Elsevier Ltd and Techna Group S.r.l. All rights reserved.
http://dx.doi.org/10.1016/j.ceramint.2013.01.106

inversion. Different synthetic routes to prepare nanocrystalline $NiFe_2O_4$ were described in the literature so far. A combustion method using various amounts of alanine as fuel has been reported by Prabhakaran et al. [4]. The role of the D,L-alanine as fuel was found to be significant in the size control and phase purity of nanocrystalline samples. Chen et al. [5] used a gel-assistant hydrothermal procedure to prepare $NiFe_2O_4$ hollow nanospheres with low saturation magnetization and high coercivity. The effects of synthetic conditions on particle sizes and magnetic properties were investigated by Li et al. [6]. The authors used hydrothermal method and pointed out the influence of the pH value, temperature and time on magnetization and coercivity.

The aim of our investigation was to study how variation of methods of synthesis influences microstructural/structural and magnetic properties of nanocrystalline nickel ferrite nanoparticles. The methods of synthesis employed in our work were based on thermal decomposition of precursors made of: (*i*) metal-nitrate salts with carboxylic acids (citric, malonic and tartaric), and (*ii*) metal-nitrate salts and polyethylene glycol (PEG) in the presence of potassium chloride as a capping agent. The as-prepared gel precursors were investigated by TGA/DTA, while the samples obtained after annealing at 450 °C were characterized by FTIR, FESEM, XRD and Mössbauer spectroscopy.

2. Experimental

2.1. Synthesis of $NiFe_2O_4$ by thermal decomposition of a precursor made of metal-nitrate salts with carboxylic acids (citric, malonic and tartaric)

After a mixture containing 0.005 mol $Ni(NO_3)_2 \cdot 6H_2O$ (Merck) and 0.01 mol $Fe(NO_3)_3 \cdot 9H_2O$ (Fluka AG) was dissolved in 100 ml of deionised water, 0.04 mol of carboxylic (citric – C; malonic – M; tartaric – T; Sigma-Aldrich) acid was added (the molar ratio of carboxylic acid per nitrate ion ions was 1:1). A 0.01 mol of KCL was finally added and the mixture was stirred at 60 °C for 2 h. The mixture first turned brown, and after that a viscous gel was formed. The solvent from the gel was evaporated at 110 °C and the gel was heated on air until self-ignited. Precursors materials obtained by this procedure were labeled as P_C, P_M and P_T, where the subscripts denote corresponding acids. Precursors materials obtained by this procedure were labeled as P_C, P_M and P_T, where the subscripts denote corresponding acids. The obtained precursor materials were heated in furnace up to 450 °C with a heating rate of 10 °C min^{-1}. Resulting powder samples were repeatedly suspended in redistilled water followed by centrifugation in order to remove residual salts. The final product was filtered and dried at 105 °C for 2 h. Precursors materials obtained by this procedure were labeled as $NiFe_C$, $NiFe_M$ and $NiFe_T$, where the subscripts denote corresponding acids.

2.2. Synthesis of $NiFe_2O_4$ by thermal decomposition of a precursor made by a reaction of metal-nitrate salts and polyethylene glycol (PEG)

Ferric oxide powders were synthesized by a slightly modified method previously described in the literature [7]. A mixture containing 0.002 mol $Ni(NO_3)_2 \cdot 6H_2O$ (Merck) and 0.004 mol $Fe(NO_3)_3 \cdot 9H_2O$ (Fluka AG) was dissolved in 50 ml of deionised water, and 0.006 mol of PEG 1550 (Fluka AG) was added in the solution. Finally, 0.018 mol of KCl was added, and the resulting transparent solution was thoroughly stirred by a magnetic mixer at 70 °C until a homogenous sol-like mixture was formed. The solvent from the mixture was evaporated at 110 °C for 2 h, and the resulting gel was heated in air until self-ignited. The obtained precursor material, labeled as P_p, was gradually heated in furnace up to 450 °C with a heating rate of 10 °C min^{-1}. Resulting powder was freed from residual salt by suspending in redistilled water followed by centrifuging. Final product was obtained by filtrating and drying at 105 °C for 2 h. Final product was obtained after filtration, and drying at 105 °C for 2 h. The obtained sample was labeled as $NiFe_{PEG}$.

2.3. Experimental methods

In order to reveal degradation behavior of the as-prepared precursors, they were studied by simultaneous thermogravimetric (TGA) and differential thermal (DTA) analysis in the range 30–800 °C using a SDT Q600 TGA/DSC instrument (TA Instruments). The heating rates were 20 °C min^{-1} and the sample masses were below 10 mg. The furnace atmosphere consisted of dry air at a flow rate of 100 cm^3 min^{-1}.

The FTIR spectra of samples (KBr pellets) were recorded in the range of 400–4000 cm^{-1} and 200–700 cm^{-1} using a Fourier transform infrared spectrometer (FTIR, model 2000, Perkin Elmer) in transmission mode at a resolution of 4 cm^{-1}. The spectra were processed using the IRDM (IR Data Manager) program.

FESEM images were recorded using a thermal field-emission scanning electron microscope, JSM-7000 F, Jeol Ltd, Japan. The FE SEM was coupled with an energy-dispersive X-ray analyzer, EDS/INCA 350, Oxford Instruments, England. The inspected samples were not coated with conductive layer.

X-ray powder diffraction (XRPD) data were collected on a PANalytical X'pert PRO diffractometer equipped with Anton Paar HTK-1200 N using CuK_α radiation. Data were collected in the 2θ range from 15.019 to 119.941° in steps of 0.067° and the total integration time of 1000 s per step (full range of the 128-channel linear RTMS detector was used, so that each channel integrated the intensity for about 7.8 s at each step).

The Mössbauer spectra were collected in a transmission configuration, in constant acceleration mode with the radioactive source of ^{57}Co embedded in Rhodium matrix.

Room temperature spectrum of α-iron foil was used for spectrometer calibration.

3. Results and discussion

3.1. Sample formation

3.1.1. The TGA/DTA of the as-prepared gel precursors

In order to study the synthesis of $NiFe_2O_4$ nanoparticles by thermolysis of corresponding precursors, simultaneous thermogravimetric (TGA) and differential thermal (DTA) analysis of the prepared precursors from ambient temperature to 800 °C were performed. The TGA and DTA curves of the as-prepared precursors P_C, P_M, P_T and P_P are shown in Fig. 1 a–d.

According to the previously proposed mechanism [8] decomposition of the citrate precursor (P_C) is expected to occur in three major steps: dehydration, decomposition of the anhydrous precursor to acetonedicarboxylate complex and decomposition of acetonedicarboxylate complex to nickel ferrite. The dehydration occurs in two not well-resolved steps (TGA curve, Fig. 1a) up to 127 and 164 °C with weight losses found 12.8 and 15.2%, respectively. The DTA curve for P_C (Fig. 1a) shows a broad endothermic peak at 125 °C due to dehydration. After dehydration, three steps in the decomposition of anhydrous precursor were observed: evolution of CO occurs up to 212 °C resulting in the formation of the acetonedicarboxylate complex $Ni_3Fe_6O_4(C_5H_6O_6)_8$ (weight loss found 20.0%). The next step corresponds to the evolution of acetone and CO_2 and takes place up to 287 °C. The residue at this stage probably has a structure related to the nickel ferrite with trapped CO_2, $Ni_3Fe_6O_{12}(CO_2)_3$ [8]. Decomposition of the $Ni_3Fe_6O_{12}(CO_2)_3$ up to 383 °C reveals the formation of the $NiFe_2O_4$ with corresponding exothermic effect at 365 °C in DTA curve due to the formation of the $NiFe_2O_4$.

TGA curve of the malonato precursor (P_M) (Fig. 1b) shows that the dehydration is finished up to 142 °C (weight loss found 5.6%) with corresponding endothermic DTA peak at 122 °C. Further decomposition step of the anhydrous precursor occurs up to 287 °C (weight loss found 33.0%) and probably corresponds to the formation of iron(III)- and nickel(II) malonate intermediates [9]. After that,three decomposition steps up to 402, 512 and 605 °C have been observed in TGA curve (Fig. 1b) (weight losses found 21.4, 6.8 and 4.0%, respectively). These steps are accompanied with three exothermic peaks in DTA curve at 339, 462 and 566 °C, suggesting the formation of the mixture of oxide phases, i.e. NiO and α-Fe_2O_3 up to 402 °C (total weight loss about 60%), $NiFe_2O_4$ and NiO phases up to 512 °C and trace of the NiO in the mixture of $NiFe_2O_4$ and NiO up to

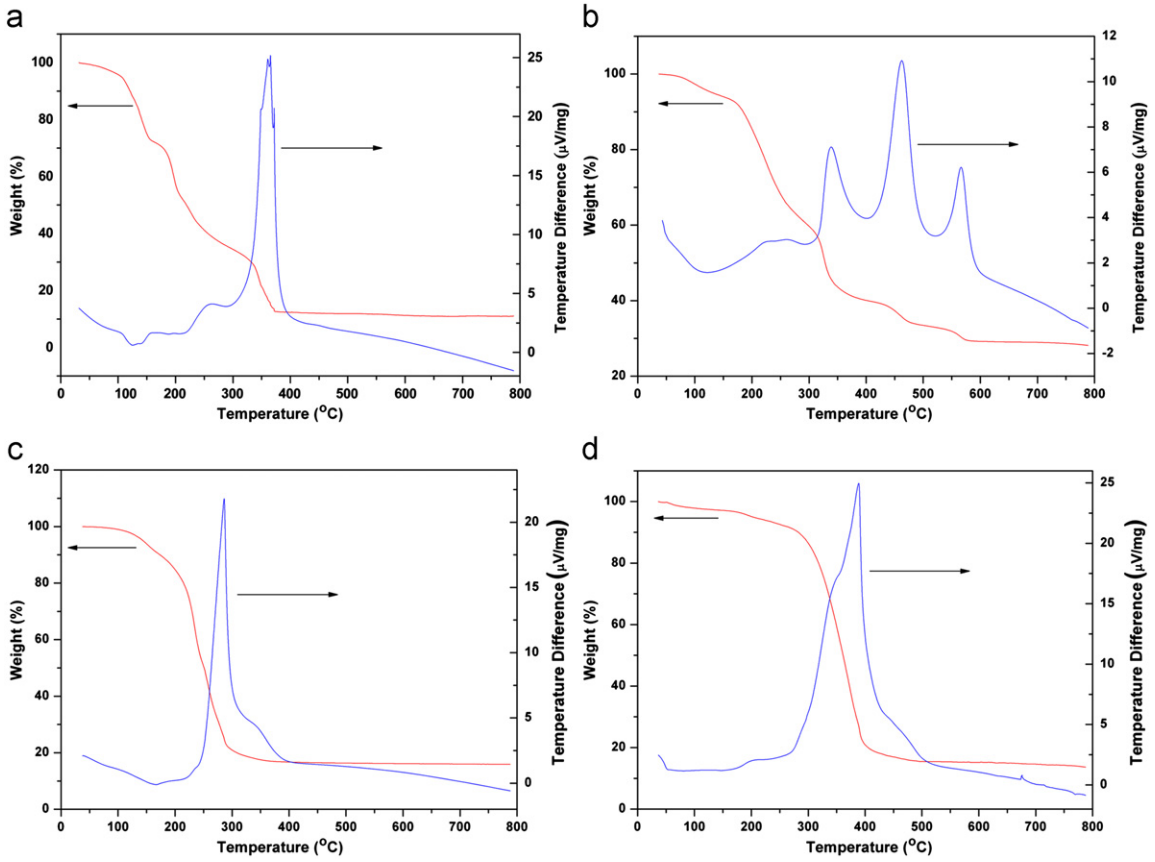

Fig. 1. TG and DTA curves of decomposition process of the citrate (a), malomato (b), tartarato (c) and PEG (d) precursors.

605 °C. This is similar to the already proposed decomposition mechanism [9].

The decomposition of the tartarato precursor (P_T) (Fig. 1c) starts with dehydration from room temperature up to 170 °C (weight loss found 9.5%) with corresponding endothermic peak in DTA curve at 167 °C due to the dehydration process. Immediately after the dehydration, two overlapped steps up to 248 and 275 °C (weight losses found 38.6 and 20.5%, respectively) could be seen in TGA curve. According to Yang et al. [10], the first step corresponds to the decomposition of iron(III) tartarate, while the second one matches to the decomposition of nickel(II) tartarate. Next, a sharp DTA exothermic peak at 286 °C together with the weight loss of 14.4% from 275 to 371 °C was observed in TGA curve, which implies the formation of some intermediates, such as α-Fe_2O_3 and NiO. This data is in agreement with the decomposition mechanism described by Yang et al. [10]. The TGA curve (Fig. 1c) clearly shows that the temperature of 371 °C corresponds to the complete decomposition of the precursor P_T to $NiFe_2O_4$ with the residual mass of about 16% at 800 °C.

The dehydration of the PEG precursor (P_P) (Fig. 1d) is a two steps process, where gel losses 1.9 and 3.9% up to 87 and 217 °C, respectively. Further decomposition of the anhydrous P_P occurs in three non-well resolved steps resulting in three overlapped steps shown in TGA curve. The first step dominates in the range 217–384 °C (weight loss found to be 64.2%). In the subsequent two steps, P_P losses 11.9 and 2.8% of its mass, up to 425 and 505 °C, respectively. These three decomposition steps correspond to the broad exothermic peak in DTA curve (Fig. 1d) with the maxima at 389 °C.

3.1.2. FTIR spectra

FTIR spectra of nickel ferrite powders obtained by combustion of carboxylic (C, M and T) acid precursors and degradation of metal nitrate salts in the presence of PEG were shown in Fig. 2. The presence of adsorbed H_2O caused the appearance of a strong and broad ν(O–H) stretching band in the 3450-3430 cm^{-1} region in the FTIR spectra of all investigated samples (Fig. 2a–d). Two shoulders at about 2920 and 2850 cm^{-1} are assigned to ν(C–H) vibrations of the citrato and the tartarato ligand, as well as of PEG in $NiFe_C$, $NiFe_T$ and $NiFe_{PEG}$ spectra, respectively. Two strong and broad bands at about 1630 and 1380 cm^{-1} are assigned to the asymmetric, ν_{as}(COO), and symmetric, ν_s(COO), stretching vibrations of the COO groups [11] are clearly seen in the FTIR spectra of $NiFe_C$ and $NiFe_M$ (Fig. 2a and b). A band at around 1630 cm^{-1} in spectra are associated with δ(HOH) vibrations of the hydroxyl group [8]. Some weak but distinct bands in the range 1000–830 cm^{-1} are assigned to ν(C–O), ν(C–C) and ν(O–H) bending modes (Fig. 2). Two broad and characteristic bands in the 606–586 and 397–417 cm^{-1} region correspond to the vibrations of metal-oxygen bond [11] in a spinel phase.

3.2. Structure/microstructure of nickel ferrite nanoparticles

3.2.1. FESEM and EDS analysis

Morphology, particle size and agglomeration of the particles were investigated by FESEM, Fig. 3a–d. In the $NiFe_C$ sample two types of particles are observed: smaller, spherical nanoparticles and bigger, cubic-like ones (Fig. 3a). Particle size distribution is pretty narrow in this sample. In sample $NiFe_M$ (Fig. 3b) small spherical nanoparticles form big agglomerates. However, a significant portion of organic phase is also observed in this sample. Nanoparticles found in the sample $NiFe_T$ are smaller than those in $NiFe_C$ and $NiFe_M$ (Fig. 3c). They are spherical in shape and very homogeneous in size and morphology. In the sample $NiFe_{PEG}$ (Fig. 3d), apart from smaller nanoparticles, presence of bigger ones, ~100 nm in size, was observed.

The samples were analyzed by EDS. The EDS spectra of two selected samples, $NiFe_T$ and $NiFe_{PEG}$, are shown in Fig. 4. When the point EDS analysis was performed, average atomic ratio of Ni to Fe is found to be very close to 1:2. The EDS analysis carried out from the surface

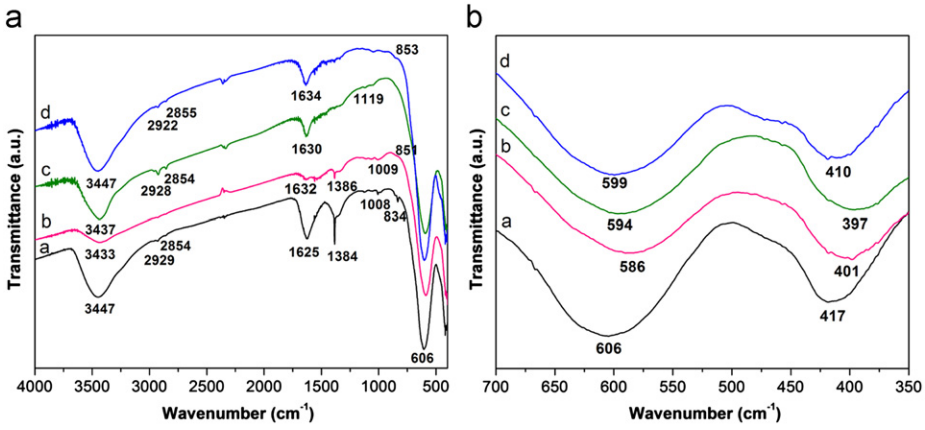

Fig. 2. The FTIR spectra of nickel ferrites: (a) $NiFe_C$, (b) $NiFe_M$, (c) $NiFe_T$ and (d) $NiFe_{PEG}$, over 4000–400 (left), and 700–350 cm^{-1} (right) wavelength range.

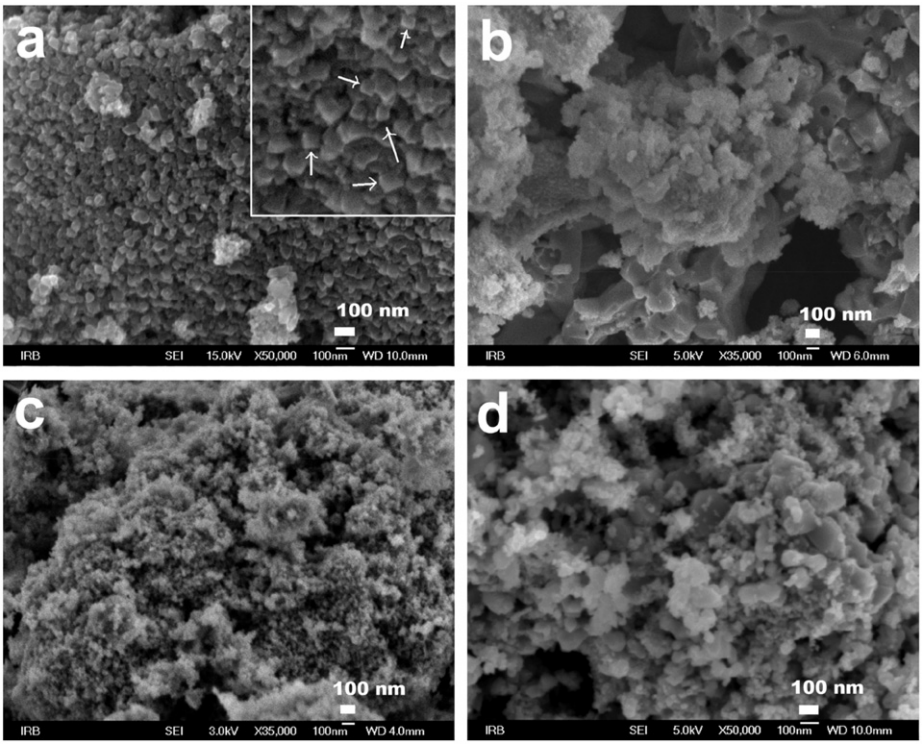

Fig. 3. FESEM images of nickel ferrites: (a) $NiFe_C$, (b) $NiFe_{M,}$ (c) $NiFe_T$ and (d) $NiFe_{PEG}$.

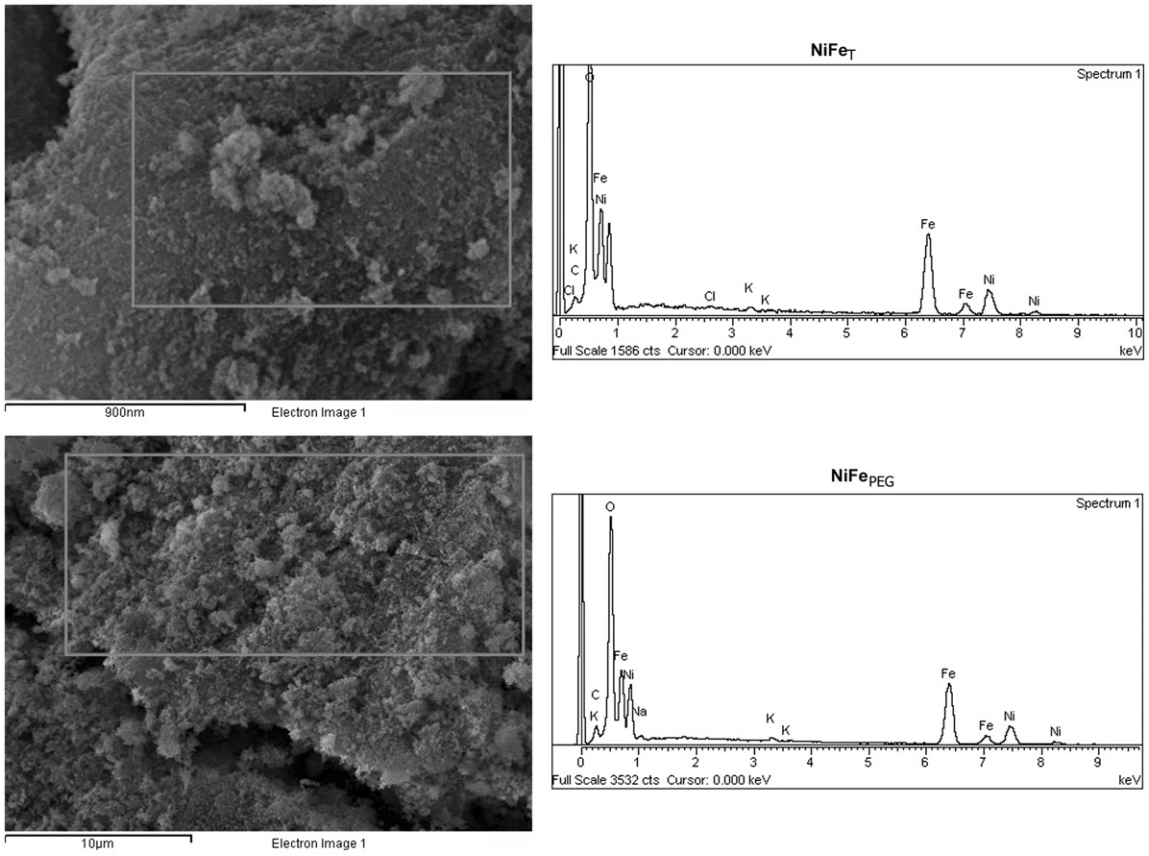

Fig. 4. EDS spectra for nickel ferrites, $NiFe_T$ and $NiFe_{PEG}$.

pointed out an excess of iron ions in the samples $NiFe_C$, $NiFe_M$ and $NiFe_{PEG}$, but not in the sample $NiFe_T$. The excess of iron ions can indicate trace of an additional phase, probably elemental iron. Such an assumption is supported by the fact that the X-ray diffraction patterns show a slight contamination of the samples by iron (Section 3.2.2.).

3.2.2. X-ray diffraction analysis

The X-ray diffraction patterns of $NiFe_C$, $NiFe_M$, $NiFe_T$ and $NiFe_{PEG}$ showed broad reflections due to their nanocrystalline structure, Fig. 5. All reflections were indexed in the spinel type of the crystal structure (space group *Fd*-3*m*). An additional reflection of small intensity, belonging to Fe at position 44.5° 2θ denoted as a contamination in all samples.

The collected X-ray diffraction data were analyzed by FullProf program by using profile matching mode [12]. The profile of diffraction peaks was described by Thompson-Cox-Hastings approximation of Voigt function comprising the size and strain calculations based on integral breadths [13]. The instrumental Full Width at Half Maximum (FWHM) was derived from XRPD pattern of standard LaB_6 powder sample for microstructure analysis. From the X-ray line broadening analysis the apparent crystallite sizes and strains were calculated for each reflection using the formula:

$$App-size = \frac{1}{\beta_{size}}\ (\text{Å}) \tag{1}$$

$$App-strain = \frac{1}{2}\beta_{strain} d_{hkl}\ (10^{-4}) \tag{2}$$

The β_{size} is obtained from the size parameters contributing to the FWHM:

$$FWHM(Lorentzian-size) = H_{LZ} = \frac{Y}{\cos\theta} \tag{3}$$

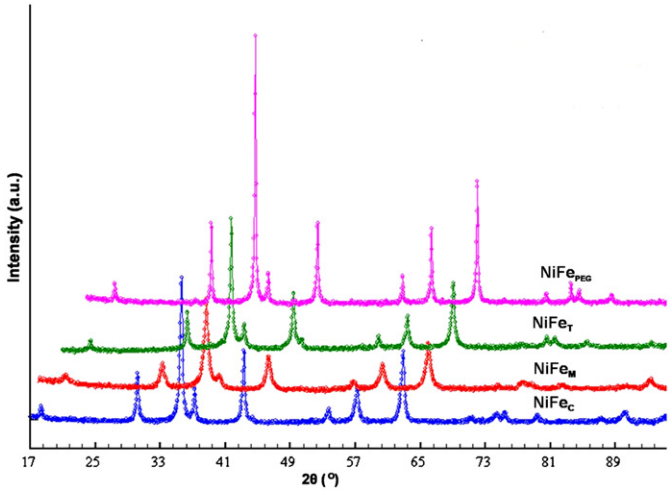

Fig. 5. X-ray diffraction patterns of nickel ferrites prepared by different routes (see text).

The β_{strain} is obtained from the strain parameters contributing to the FWHM:

$$FWHM^2(Gaussianstrain) = H_{GS}^2 = (U + (1\xi)^2 D_{ST}^2(\alpha_D))\tan^2\theta \tag{4}$$

$$FWHM(Lorentzian-strain) = H_{LS} = (X + \xi D_{ST}(\alpha_D))\tan\theta \tag{5}$$

Both β_{size} and β_{strain} are deduced from TCH parameters according to the procedure described previously [14]. The standard deviations appearing in the global average apparent size and strain is calculated using the different reciprocal lattice directions.

The values of cell parameters and microstructure (apparent crystallite size and average microstrain) are summarized in Table 1. Crystallite size was found to be between 11 and 16 nm for samples $NiFe_C$, $NiFe_M$, and $NiFe_T$, and 33 nm for $NiFe_{PEG}$. No significant variation in crystallite size with change of carboxylic acid (C, M and T) in precursor material was observed, but samples prepared in the presence of PEG yielded larger crystallites, Table 1. As expected, average strain decreases as the crystallite size increases.

Significant differences in lattice parameters (Table 1) result from changes in cation distribution, nonstoichiometry and presence of structural imperfections in nickel ferrite nanoparticles. The distribution of cations at the crystallographic positions (8*a* and 16*d* in the spinel structure type) in the nanocrystalline nickel ferrite is mixed as it was already reported by many authors [15]. The Fe^{3+} and Ni^{2+} ions have no exclusive preference for tetrahedral or octahedral sites, and can fill both sites. However, the differences in ionic radii of cations are significant when they populate octahedral (16*d*) and tetrahedral (8*a*) positions. Therefore, specific cationic distribution affects the cation–anion distances and therefore the lattice parameter values.

3.3. Mössbauer spectra analysis

The ^{57}Fe Mössbauer measurements were performed on the samples, $NiFe_M$, $NiFe_T$ and $NiFe_{PEG}$. Mössbauer spectra of nickel ferrite nanopowders (Fig. 6) show a superposition of two sextet lines (refer to a magnetic contribution) and a quadrupole doublet (characteristic of a paramagnetic phase) [16]. The refined hyperfine parameters of samples are reported in Table 2. According to

Table 1
Unit cell, apparent crystallite size and average strain for nickel ferrites. Estimated standard deviations are in parentheses.

Sample	*Lattice parameter (Å)*	*Crystallite Size (nm)*	*Strain (10^4)*
$NiFe_C$	8.3574 (2)	15	18
$NiFe_M$	8.3417 (2)	11	12
$NiFe_T$	8.3369 (2)	16	9
$NiFe_{PEG}$	8.3408 (1)	33	1

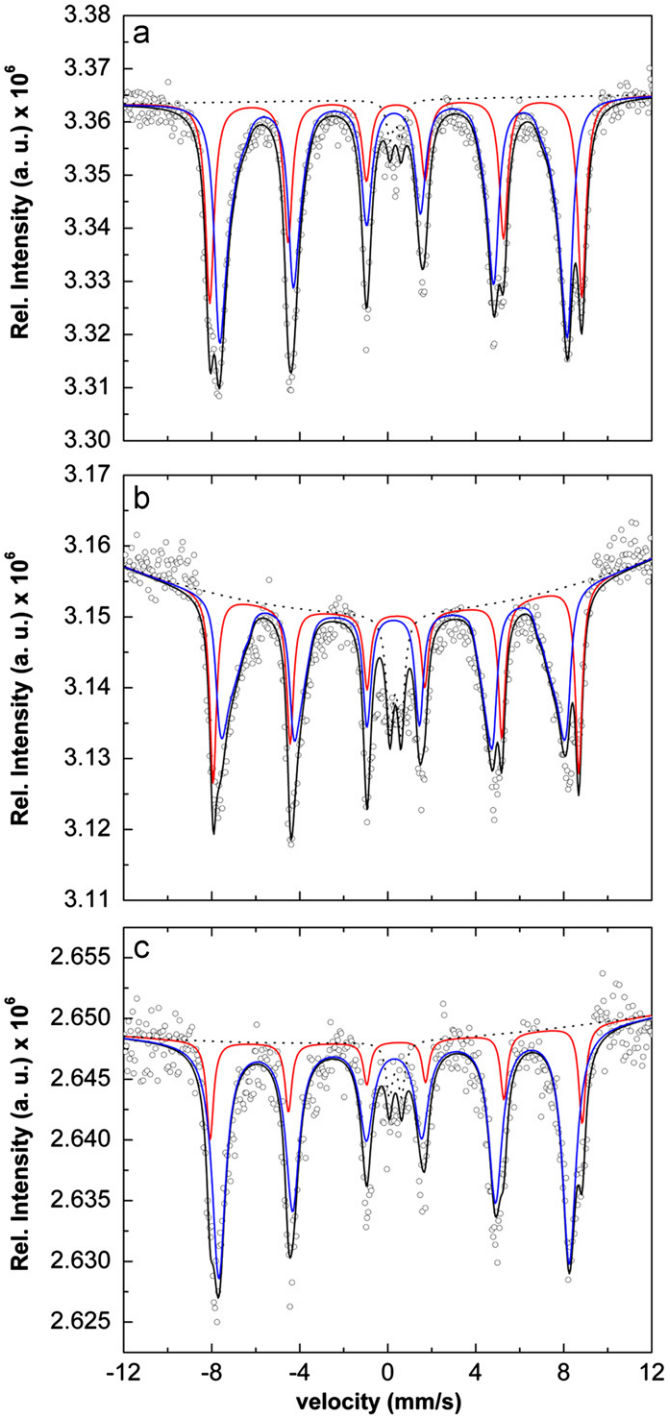

Fig. 6. Room temperature Mössbauer spectra of nickel ferrites: (a) $NiFe_M$, (b) $NiFe_T$ and (c) $NiFe_{PEG}$.

the values of the isomer shift and hyperfine field at room temperature, the two sextets are attributed to tetrahedral (A) and octahedral (B) iron sites in the spinel lattice. These results are in good agreement with literature data for nanosize $NiFe_2O_4$ [17,18]. Due to small particles size, non-stoichiometry, structural and magnetic imperfections, the obtained hyperfine field values in investigated nanosize samples (Table 2) are lower than those found for bulk counterpart (B_{hf}(A) = 50.6 T; B_{hf}(B) = 54.8 T) [16]. This

Table 2
Hyperfine parameters: IS—isomer shift; B_{hf}—hyperfine field, QS–quadrupole splitting; Γ—linewidth, and A—relative spectral area (%), obtained from refinement of Mössbauer spectra of nanocrystalline nickel ferrites. Errors: IS = ± 0.01 mm/s; QS = ± 0.01 mm/s; Γ = ± 0.01 mm/s; B_{hf} = ± 0.2 T and A = ± 1%.

Sample	*Component*	*IS (mm/s)*	B_{hf} *(T)*	*QS (mm/s)*	Γ *(mm/s)*	*A(%)*
$NiFe_M$	Sextet A	0.26	47.8	–	0.50	63
	Sextet B	0.37	52.4	–	0.46	35
	Doublet	0.35	–	0.50	0.36	2
$NiFe_T$	Sextet A	0.25	46.5	–	0.39	57
	Sextet B	0.38	51.5	–	0.37	33
	Doublet	0.35	–	0.50	0.38	10
$NiFe_{PEG}$	Sextet A	0.29	49.4	–	0.74	79
	Sextet B	0.38	52.5	–	0.37	17
	Doublet	0.35	–	0.55	0.36	4

depression is more expressed in samples $NiFe_M$ and $NiFe_M$ with smaller particles (see FESEM images, Fig. 3), while the sample NF_{PEG} has the highest hyperfine field values which correspond to a better crystallization. The average hyperfine field value for tetrahedral site $\langle B_{hf}(A) \rangle$ in samples $NiFe_M$ and $NiFe_T$ is obtained taking into account hyperfine field distribution. The broad sextet lines (the large linewidths) indicate great distortion of A and B sites. The superparamagnetic contribution is the highest in sample $NiFe_T$ with the smallest nanoparticles. The quadrupole splitting of a superparamagnetic doublet has similar values in all three samples.

4. Summary

Nanocrystalline nickel ferrites were synthesized from a precursors obtained from metal-nitrate salts and either carboxylic acid (citric, malonic, or tartaric acid) or polyethylene glycol. Thermal decomposition of precursors was analysed by TGA/DTA measurements and these analyses indicate the formation of nickel ferrites. All precursors were annealed at the same temperature of 450 °C in order to investigate the influence of applied method on structural, microstructural and magnetic properties. The differences in the values of lattice parameters are closely related to differences of preparation methods. Microstructural parameters were similar in combustion methods with different carboxylic acids, but significantly different from values in PEG assisted synthesis. The nanosized effects (superparamagnetism and local distortions) are clearly expressed on the magnetic properties.

Acknowledgment

The Serbian Ministry of Science, Technology and Development supported this work financially, projects Grant nos. III45015, 172035 and III45007.

References

[1] G.F. Goya, V. Grazú, M.R Ibarra, Magnetic nanoparticles for cancer therapy, Current Nanoscience 4 (2008) 1–16.

[2] A. Goldman, Modern Ferrite Technology, Marcel Dekker, Inc., New York, 1993.

[3] J.G. Na, T.D. lee, S.J. Park, Y. Tang, H.L. Luo, Effects of cation distribution on superexchange interaction in cobalt ferrites, IEEE Transactions on Magnetics 31 (1995) 3970–3972.

[4] T. Prabhakaran, J. Hemalatha, Combustion synthesis and characterization of highly crystalline single phase nickel ferrite nanoparticles, J. All. Compd. 509 (2011) 7071–7077.

[5] L. Chen, H. Dai, Y Shen, J. Bai, Size-controlled synthesis and magnetic properties of $NiFe_2O_4$ hollow nanospheres via a gel-assistant hydrothermal route, J. All. Compds. 491 (2010) L33–L38.

[6] H. Li, H-z. Wu, G-x. Xiao, Effects of synthetic conditions on particle size and magnetic properties of $NiFe_2O_4$, Powder Technology 198 (2010) 157–166.

[7] J. Song, Z-Y. Ma, C. Li, R-J. Wu, Synthesis of ferric oxide nanoparticles with controllable crystal phases by salt-assisted combustion method, Journal of Inorganic Materials 25 (7) (2010) 780–784.

[8] N.S. Gajbhiye, S. Prasad, Thermal decomposition of hexahydrated nickel iron citrate, Thermochimica Acta 285 (1996) 325–336.

[9] B.S. Randhawa, J. Singh, H. Kaur, M. Kaur, Preparation of nickel ferrite from thermolysis of nickel tris(malonato)ferrate(III) heptahydrate precursor, Ceramics International 36 (2010) 1993–1996.

[10] J.M. Yang, W.J. Tsuo, F.S. Yen, Preparation of Ultrafine nickel ferrite powders using mixed Ni and Fe tartartes, Journal of Solid State Chemistry 145 (1999) 50–57.

[11] K. Nakamoto, Infrared and Raman Spectra of Inorganic and Coordination Compounds, Part B, Applications in Coordination, Organometallic and Bioinorganic Chemistry, 5th ed., John Wiley & Sons, New York, 1997.

[12] J. Rodriguez-Carvajal, FullProf computer program 〈http://www.ill.eu/sites/fullprof/〉 (2009).

[13] J. Rodríguez-Carvajal, Recent developments of the program FULLPROF, in commission on powder diffraction (IUCr), Newsletter 26 (2001) 12–19.

[14] 〈http://www-llb.cea.fr/fullweb/fp2k/fp2k_divers.htm〉.

[15] A. Ahlawat, V.G Sathe, V. . Reddy, A. Gupta, Mossbauer, Raman and X-ray diffraction studies of superparamagnetic $NiFe_2O_4$ nanoparticles prepared by sol–gel auto-combustion method, Journal of Magnetism and Magnetic Materials 323 (2011) 2049–3054.

[16] N.N. Greenwood, T.G. Gibb, Mössbauer Spectroscopy, Chapman and Hall, London, 1971, p. 266.

[17] S. Prasad, N.S. Gajbhiye, Magnetic studies of nanosized nickel ferrite particles synthesized by citrate precursor technique, Journal of Alloys and Compounds 265 (1998) 87–92.

[18] C.N. Chinnasamy, A. Narayanasamy, N. Ponpandian, K. Chattopadhyay, K. Shinoda, B. Jeyadevan, K. Tohji, K. Nakatsuka, T. Furubayashi, I. Nakatani, Mixed spinel structure in nanocrystalline $NiFe_2O_4$, Physical Review B 63 (2001) 184108 (6 pp).